Laminated Ti-Al composites: processing, structure and strength

Yan Du, Guohua Fan, Tianbo Yu, Niels Hansen, Lin Geng, Xiaoxu Huang

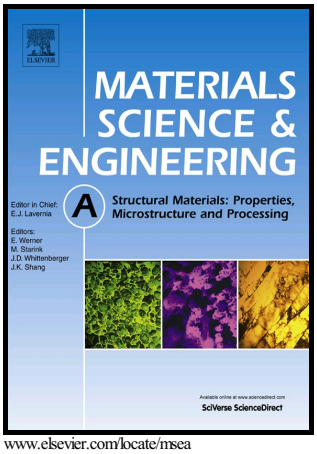

www.elsevier.com/locate/msea

PII: S0921-5093(16)30883-8
DOI: http://dx.doi.org/10.1016/j.msea.2016.07.108
Reference: MSA33939

To appear in: *Materials Science & Engineering A*

Received date: 25 May 2016
Revised date: 25 July 2016
Accepted date: 26 July 2016

Cite this article as: Yan Du, Guohua Fan, Tianbo Yu, Niels Hansen, Lin Geng and Xiaoxu Huang, Laminated Ti-Al composites: processing, structure and strength, *Materials Science & Engineering A* http://dx.doi.org/10.1016/j.msea.2016.07.108

Laminated Ti-Al composites: processing, structure and strength

Yan Du[a,b], Guohua Fan[a]*, Tianbo Yu[b], Niels Hansen[b], Lin Geng[a] and Xiaoxu Huang[b]

a. School of Materials Science and Engineering, Harbin Institute of Technology, Harbin, 150001 Harbin, China

b. Section for Materials Science and Advanced Characterization, Department of Wind Energy, Risø Campus, Technical University of Denmark, DK-4000 Roskilde, Denmark

Corresponding author: G.H. Fan; E-mail: ghfan@hit.edu.cn

Abstract

Laminated Ti-Al composite sheets with different layer thickness ratios have been fabricated through hot pressing followed by multi-pass hot rolling at 500˚C. The laminated sheets show strong bonding with intermetallic interface layers of nanoscale thickness between the layers of Ti and Al. The mechanical properties of the composites with different volume fractions of Al from 10% to 67% show a good combination of strength and ductility. A constraint strain in the hot-rolled laminated structure between the hard and soft phases introduces an elastic-plastic deformation stage, which becomes more pronounced as the volume fraction of Al decreases. Moreover, the thin intermetallic interface layer may also contribute to the strength of the composites, and this effect increases with increasing volume fraction of the interface layer.

Keywords: electron microscopy; mechanical characterization; composites; thermomechanical processing; interfaces

1. Introduction

Development of new and advanced metallic materials with high strength and good toughness is a common goal in a global effort [1, 2]. However, the toughness of metals typically decreases with increasing strength. Metal Matrix Composites (MMCs) offer a unique opportunity to combine strength and toughness with good impact and fracture resistance [3-5]. Therefore, MMCs have been

investigated extensively and different structural morphologies have been explored [6], such as network [7], gradient [8, 9], shell-core [10] and laminate [5, 11, 12]. The laminated metal composites (LMCs) have been investigated since the 1990s [13-15]. In recent years, however, LMCs have attracted significant attention not only due to a good combination of ductility, strength and density, but also because of an excellent damping capacity required in light weight vehicles [16-18]. Multiple systems such as Cu/Nb, Al/Zn and Al/Ti fabricated by accumulative roll bonding and asymmetric accumulative roll bonding at room temperature have been investigated emphasizing mechanical properties and microstructure [19-21]. However, the stress states in LMC sheets during rolling are complex and stress localization between component layers can lead to severe local necking. According to recent studies of LMCs hot rolled [22, 23] or hot pack rolled [24], the local shear of the component layers decreases with increasing rolling temperature and our previous study [25] has also shown that homogenous reduction of layers can be obtained for laminated Ti-(SiC_p/Al) composites by hot pressing followed by hot rolling.

Since Ti and Al are strong and light, respectively, it is of great interest to study laminated Ti-Al composites for applications in the automobile and aerospace industries. In previous studies of this system, LMCs were obtained by accumulative roll bonding or direct hot roll bonding to a thickness reduction of 50% [21, 32]. However, the resultant microstructure is heterogeneous, showing local necking, and therefore its tensile ductility is low (1.5~22 % under different conditions) [21]. In order to produce laminated Ti-Al composites with uniform thickness reduction of component layers without local necking, hot pressing followed by hot rolling was applied in our previous work [26]. Also the interfaces of the hot-rolled laminated Ti-Al composites have been characterized in a scanning electron microscope (SEM) equipped with an electron backscatter diffraction (EBSD) facility. It has been observed that a rough interface creates structural heterogeneities, which affects the annealing behavior of the LMCs [26]. Other previous studies also show that interface

heterogeneities [33] and interface-facilitated deformation exist in LMCs [34]. The presence of this interface layer between Al and Ti may also affect the mechanical properties, which are investigated in this study, where LMCs with five different Ti/Al layer thickness ratios were fabricated using commercial purity Ti and Al sheets. The microstructures of these materials were characterized, and the mechanical properties were examined by tensile testing. The data were analyzed to answer the following questions:

i) Do the LMCs have properties which point to further development for industrial applications?

ii) Can the experimental stress-strain behavior be modelled by applying a general rule of mixture (ROM)?

iii) In the case of a difference between the ROM modelling and the experiment, what can the cause(s) be?

2. Materials and methods

2.1 Materials

Commercial purity titanium TA1 sheets with a purity of 99.4 wt% from Tianrui Non-ferrous Metal Co., Ltd. (Baoji, China), and commercial purity aluminum 1060 O sheets with a purity of 99.2 wt% from Northeast Light Alloy Co., Ltd. (Harbin, China) were selected as raw materials. The chemical compositions and materials mechanical and physical properties are given in Tables 1 and 2. Ti sheets with a thickness of 200 μm and Al sheets with thicknesses of 400 μm, 200 μm, 100 μm, 50 μm and 20 μm were used as the starting materials to produce LMCs with different thickness ratios between Ti and Al. All the sheets were cut into small pieces with a dimension of 100 mm × 100 mm.

2.2 Fabrication process

The hot-rolled LMCs were produced in three steps. i) Sheet preparation: the Ti and Al sheets were treated by 10 vol.% HF and 10 vol.% NaOH, respectively, to remove contaminants and oxide layers from the surfaces. Then, the treated sheets were roughened with a steel brush, cleaned in an

ultrasonic bath with acetone for 5 min, and dried. ii) Diffusion bonding: the sheets were stacked alternately to about 6 mm in thickness with Ti sheets at the top and the bottom, put into a graphite die to confine the stack, and pressed at 500˚C for 1 h under a pressure of 40 MPa in a vacuum hot pressing furnace to obtain hot-pressed LMCs with a total thickness of about 6 mm. iii) Hot rolling: The hot-pressed LMCs were hot rolled with a thickness reduction of 50% to about 3 mm. The details of the rolling condition have been given elsewhere [26], and the schematic of the fabrication process is shown in the supplementary material 1 (S1). Materials parameters of the hot-rolled LMCs are shown in Table 3.

2.3 Characterization

The microstructure and texture of the hot-rolled LMCs were characterized by a SEM (Zeiss Supra 35) equipped with an automated HKL EBSD facility. The sample surfaces for observation were the normal direction-transverse direction (ND-TD) planes. The samples were prepared by mechanical polishing for backscatter electron (BSE) imaging and electro polishing for EBSD mapping. The step size of EBSD data was 2 μm. A detailed study on the interface of the LMCs was carried out using a transmission electron microscope (TEM, Tecnai G2 F30). A thin foil revealing the normal direction-rolling direction (ND-RD) section for TEM observation was prepared by an FEI HELIOS Nanolab 600i dual-beam workstation. Uniaxial tensile tests of the LMCs were carried out using an Instron-5569 universal testing machine. An extensometer with a gauge of 10 mm was applied to dog bone shape tensile specimens of LMCs with gauge dimension of 18 mm × 5 mm × 3 mm. Dog bone shape tensile specimens of Ti and Al sheets, which had been under the same hot rolling condition as the LMCs, were also prepared and tested. The thicknesses of Ti and Al sheets were 3 mm and 100 μm, respectively. A total of three specimens for each material conditions were tested at a constant crosshead speed of 2 mm/min (corresponding strain rate of $1.8E^{-3}$ s^{-1}). Both engineering stress/strain and true stress/strain curves were obtained from the database of the testing

machine. The Vicker's hardness of Ti and Al in different LMCs (R200, R100, R50, R25 and R10) was measured with loads of 50 g and 10 g, respectively.

3. Results

3.1 Mechanical properties of hot-rolled LMCs

Fig. 1 shows tensile engineering stress-strain curves of the R100 (see Table 3) along the TD and the RD as an example. The yield strength (YS), ultimate tensile strength (UTS) and uniform elongation (UE) of the TD and RD samples are similar with values of 172MPa, 250 MPa and 5.6%, respectively. However, the total elongation (TE) of the TD samples is about 40%, significantly higher than the elongation of the RD samples (~30%). Therefore, the TD was selected as the loading direction in the following tensile tests.

The tensile engineering stress-strain curves of individual hot-rolled Al and Ti, and hot-rolled laminated Ti-Al composites (R200, R100, R50, R25 and R10) are shown in Fig. 2. The theoretical elastic moduli of the composites have been calculated by the ROM and are shown in Table 3. The YS, UTS, TE, and UE have been obtained directly from the tensile curves, as the stress at 0.2% off-set, the maximum stress, the fracture strain and the strain at the maximum stress, respectively. These properties are given in Table 4 showing that: i) the YS and the UTS increase with decreasing Al layer thickness; ii) the YS of R10 and Ti are identical although R10 is expected to be lower; iii) the TE is 30~40% for all the LMCs; iv) the UE is in the range of 5~6% for LMCs with a volume fraction of Al from 33.3% to 66.7%, but decreases to 3~4% when the volume fraction of Al decreases to below 33.3%. This combination of strength and ductility in the LMCs is interesting, as it widens the application potential of the composites, which will be discussed in Section 5.

The hardness of Ti was independent of the thickness ratio with a mean value of 165 HV, whereas the hardness of Al was slightly dependent on the thickness ratio (increasing from 28.5±0.3 HV to 29.2±0.1 HV with decreasing Al layer thickness). Since the strength of Al and Ti can be evaluated

by their hardness, it follows that the strength of Al and Ti does not change much in all the composites with different layer thickness ratio.

3.2 Microstructure of the hot-rolled LMCs

The microstructure of the LMCs was examined by SEM. Fig. 3(a) shows a BSE image of a hot-pressed composite with a Ti/Al thickness ratio 1:1. BSE images of samples R200, R100, R50, R25 and R10 are shown as Fig. 3(b)-(f). The interface between Ti and Al layers was flat after hot pressing and became rough after hot rolling, but no reaction layer between Al and Ti was found by SEM. The Ti and Al layers deformed uniformly during the multi-pass hot rolling and no local necking occurred as shown in Fig. 3. The microstructure and texture of R100 were characterized by EBSD as shown in Fig. 4. Fig. 4(a) shows the deformed microstructure of Al and Ti layers. The Al layers have a random texture, whereas the Ti layers show a strong basal plane texture, as shown in Fig. 4(b) and (c), respectively.

The microstructure of R100 observed by TEM is shown in Fig. 5(a) for Al and Fig. 5(b) for Ti. Both structures are subdivided by dislocation cell boundaries and sub-grain boundaries with some dislocations and dislocation tangles between the boundaries. The structural scale is comparable in Ti and Al with a boundary spacing of 1 μm and 2 μm, respectively. When the melting points of Al (660 ˚C) and Ti (1668 ˚C) are taken into account, the two microstructures can be categorized as a typical hot-deformed structure and a warm-deformed structure, respectively. The microstructure of the interface region between Al and Ti has been discussed in more detail in our previous work [26]. It was demonstrated that interface roughness developed during the rolling due to different properties of the grains in Ti and Al. Protrusions and retrusions were formed along the interface, introducing areas of strain localization in the Al layer near the Ti-Al interface.

3.3 Interface in the hot-rolled LMC

Detailed TEM investigations were carried out to study the interface in the LMCs. Fig. 6 shows a

TEM micrograph at the interface of R100. Based on the micro-diffraction patterns, the $TiAl_3$ phase with a DO_{22} structure was found at the interface between Al and Ti. The thickness of the interface intermetallic phase was about 100 nm.

A line scan across the interface between Al and Ti in R100 was performed as illustrated in Fig. 7(a). Quantitative X-ray energy dispersive spectroscopy (EDS) revealed the change of chemical composition across the interface and the formation of $TiAl_3$ at the interface as shown in Fig. 7(b). Ti and Al started to diffuse during hot pressing, and it continued during the multi-pass hot rolling step. $TiAl_3$ has a lower Gibbs free energy compared to TiAl and Ti_3Al according to thermodynamic calculation presented in [27], which leads to the dominance of $TiAl_3$ in the interface layers. Interface layers of other samples showed that the thickness of the intermetallic interface is nearly the same, demonstrating that the formation of the intermetallic phase is independent of the Ti/Al layer thickness ratio. However, the thickness of the intermetallic layer may be controlled by choosing hot-rolling conditions including number of rolling passes, thickness reduction and rolling temperature, which is for future research and development.

4. Discussion

4.1 Rule of Mixture

The strength of the composites can be estimated by applying the ROM [13, 15]. According to the hardness of Ti and Al layers in the LMCs, their individual flow stress does not change significantly with layer thickness ratio. Thus, the tensile stress-strain behavior of the composites can be calculated based on the tensile stress-strain curves of hot-rolled Ti and Al. In this case, the analysis requires: i) the tensile stress-strain curves of hot-rolled Ti and Al, and ii) the volume fractions of Ti and Al. The application of the ROM has been based on the following assumptions:

i) The deformation is uniform throughout the composite and the elastic/plastic strains of Ti and Al are identical to the external strain during deformation, i.e $\varepsilon_{Ti}=\varepsilon_{Al}=\varepsilon$.

ii) The strength of Ti in the LMCs is identical to that of hot-rolled Ti with a thickness reduction of 50%. The flow stress of Ti is measured up to a strain corresponding to the UTS, and at larger strains the work hardening rate is negligible and the flow stress is taken to be constant.

iii) The strength of Al in the LMCs is identical to that of hot-rolled Al with a thickness reduction of 50%, and the tensile behavior of the Al foil is assumed to be independent of the thickness.

Based on the above idealized assumptions, the flow stress of the composites with different layer thickness ratios at a given strain can be obtained on the basis of the ROM:

$$\sigma = \sigma_{Ti} \cdot \nu_{Ti} + \sigma_{Al} \cdot \nu_{Al} \quad (1)$$

and

$$\nu_{Ti} + \nu_{Al} = 1 \quad (2)$$

where σ is the flow stress of the composite, σ_{Ti} and σ_{Al} are the flow stresses of hot-rolled Ti and Al, and υ_{Ti} and υ_{Al} are the volume fractions of Ti and Al as shown in Table 3. The flow stress is obtained from the true stress-strain curves of Ti and Al at given strains as shown in Fig. 8(a). The dashed line for Ti illustrates the assumption of a constant flow stress. A tensile flow curve can be obtained corresponding to successive strains and the work hardening rate can be calculated by differentiating the flow curve, see Fig. 8(a) for R100 as an example. The uniform strain ε_u in a calculated flow curve can be determined according to the Considére criterion [28] as the strain where the work hardening rate Θ equals the stress σ, see Fig. 8(a). The corresponding stress is taken to be the UTS. It is worth noting that both Al and Ti continue to be hardened after the UTS until the work hardening rate reaches zero or the specimen fails. The calculated true tensile curves (up to a strain of 0.05) of the LMCs with different layer thickness ratios are shown in Fig. 8(b). The calculated strength of the composites increases with decreasing volume fraction of Al at all strains. The calculated mechanical property parameters are shown in Table 5, compared with the experimental properties from Table 4. For the YS, the true stress of experimental result is defined as the same as the engineering stress due to a very low area reduction in cross-section. The comparison shows a

good agreement between experimental and calculated results using the ROM for R200, R100 and R50. However, discrepancies are found for R25 and R10. For the UTS, the experimental result is the true stress (considering an area reduction in cross-section) at the UE (see Table 4). The comparison shows fewer and smaller deviations (percentage) than that for the YS. It is worth noting that strain range below 0.05 is the main region for our investigation on strengthening mechanisms in the LMCs.

4.2 Variation from Rule of Mixture

The difference between the experimental and calculated flow curves is significant for R25 and R10, whereas there is a good agreement for LMCs with thicker Al layers and higher volume fractions of Al. The variation from the ROM may have many causes and three of them will be discussed in the following. It has been characterized previously that the interface after hot deformation is rough with protrusions and retrusions [26]. This roughness may introduce some strain incomparability but the effect on strength is assumed to be small. A more significant effect is expected from two other strengthening mechanisms, which may increase the experimental strength above that calculated based on the ROM. These mechanisms relate to: (i) the formation of an interface reaction layer between Ti and Al, and (ii) a constraint effect due to different elastic/plastic behavior of Ti and Al.

4.2.1 Interface reaction layer

Since the nanoscale intermetallic phase of $TiAl_3$ forms layers at the interfaces, the strength of $TiAl_3$ should also be considered in order to calculate the strength of the LMCs. Two aspects have to be considered in this calculation: i) the effect of the interface layer of $TiAl_3$ and ii) the effect of a chemical diffusion region in Ti and Al near the interface.

The thickness of the $TiAl_3$ layer is a constant with an average value of 100 nm. Since the volume fraction of the interface phase ($TiAl_3$) can be calculated as:

$$v_{TiAl_3} = \frac{d_{TiAl_3}}{d} \tag{3}$$

where d_{TiAl_3} and d are the total thicknesses of the $TiAl_3$ layers and the LMC, respectively. A modified rule of mixture (MROM) on the strength of the LMC is therefore suggested as follows:

$$\sigma_{MROM} = \sigma_{TiAl_3} \cdot v_{TiAl_3} + \sigma_{cal.(Ti-Al)} \cdot v_{Ti-Al} \tag{4}$$

where $\upsilon_{Ti\text{-}Al}$ and υ_{TiAl3} are the volume fractions of Ti and Al metallic layers and $TiAl_3$ intermetallic layers, respectively; $\sigma_{cal.(Ti\text{-}Al)}$ is the strength of the LMC calculated by the ROM assuming that there is no intermetallic phase in the LMC; σ_{TiAl3} is the strength of $TiAl_3$; σ_{MROM} is the strength of the LMC considering interface strengthening. Since the failure stress of bulk $TiAl_3$ is around 600 MPa with a large variation due to the brittle nature of $TiAl_3$ [29], the strength of $TiAl_3$ in the LMC is calculated based on our previous work [30], showing that a $TiAl_3$ layer with a thickness of 5 μm has an elastic module of 220±10 GPa measured by nanoindentation. Here, σ_{TiAl3} is assumed to be as high as 6600±300 MPa based on an assumption of elastic deformation of $TiAl_3$ to a strain of 0.03. Thus, a variation between the calculated results based on the MROM and the ROM is expected, and this variation will increase with decreasing Al layer thickness due to increasing volume fraction of $TiAl_3$. Maximum contributions from $TiAl_3$ in the LMCs have been calculated as shown in Table 6, assuming that the strength of $TiAl_3$ is 6600±300 MPa. It is worth noting that the strength of $TiAl_3$ may be lower than 6600 MPa, and thereby the contribution from $TiAl_3$ may be smaller than the estimate. Thus, the interface reaction layer produces only small variations to the ROM.

4.2.2 Constraint effect

Due to different elastic/plastic properties of Al, Ti and the interface reaction layer, a constraint strain is expected to be developed when the LMC is strained in tension. In the first stage, both Al and Ti layers deform elastically. At a higher strain, Al deforms plastically while Ti continues to deform elastically. Finally, in the third stage, both Al and Ti deform plastically. In the second stage,

a misfit strain increases with the tensile strain and this misfit strain can be relaxed by formation of geometrically necessary dislocations [31]. These dislocations will strengthen the Al phase and increase its work hardening rate, and thus the experimental flow curve of the LMC will be above the ROM curve. As Al is constrained between the harder Ti layers, it must be expected that the constraint effect will increase with decreasing thickness of the Al layers. The constraint effect is illustrated in Fig. 9, showing that it is significantly larger in R10 than in R100. Fig. 9 also shows that this contribution to the composite strength is exhausted at a strain of about 0.015, after which the ROM is applicable. This kind of constraint effect has also been found in bulk metal material with gradient structure [35, 36], and it shows that the strain gradient will promote the formation of geometrically necessary dislocations and result in extra strain hardening. In the present case, the constraint effect results from different properties of component layers in the LMC, and therefore this effect can be better controlled by designing the component layers. Moreover, the interface interacts with dislocation movement and thus local hardening can be controlled by adjusting the interface spacing.

5. Optimization of the mechanical properties of LMCs

LMCs are engineering materials and therefore the development of the Ti/Al LMC has an objective to develop a strong and light metallic material for applications in the automobile and aerospace industries. A number of properties have to be considered and three of them are discussed in the following.

(i) The strength, which has been shown to be strongly dependent on the thickness ratio between Ti and Al, offers a possibility of material design based on properties of both materials and application of the ROM (Examples are R200, R100 and R50).

(ii) The ductility and formability are promising and the total elongations for all the composites are 30~40%, similar to those of Ti and Al. Also important is the uniform elongation, which is 5~6%

for R200, R100 and R50.

(iii) The weight, which is reduced due to the application of Al with a low density, decreases the weight per unit of the composites.

An important parameter is the specific strength:

$$\sigma_{specific} = \frac{\sigma}{\rho} \tag{5}$$

where ρ is the density. Table 7 gives the specific YS, the specific UTS, and the density of the five LMCs. Since the volume fraction of $TiAl_3$ is very low, the results were calculated based on the experimental data given in Table 4 according to the universal ROM. The specific strengths for the five LMCs are plotted in Fig. 10 together with the uniform elongation. Values for Ti are also included. This figure illustrates that a good combination of properties is obtained when the fraction of Al is in the range of 33~66%. The best specific strength is obtained for R25 and R10, where the fraction of Al is in the range up to 20%. The uniform elongation is low but it is combined with a high total elongation, which may have a beneficial effect when formability is evaluated, which is part of the ongoing investigation.

6. Conclusions and outlook

Laminated Ti-Al composites (LMCs) have been fabricated by hot pressing followed by multipass hot rolling at 500˚C. The LMCs are fully dense and show a good combination of strength, density and ductility with total elongation of 30~40% for all the composites. The key parameter is the Ti/Al layer thickness ratio and the conclusions are the following:

1) For the layer thickness of Al larger than 25 μm (Al 20 vol%), the stress-strain curves can be analyzed by applying the Rule of Mixture (ROM).

2) For a layer thickness of Al at 25 μm and below, the ROM underpredicts the flow stress by about 10% and the stress-strain curves show an elastic-plastic stage followed by plastic deformation.

3) Causes of the ROM underprediction have been identified as follows in an increasing order of

importance: i) roughness of the Ti/Al interface, ii) interface reaction between Al and Ti, iii) evolution of a constraint strain.

In an outlook, it is suggested to optimize the LMCs design by replacing the pure metals with alloys and by expanding formability studies for applications of LMCs. The constraint strain effect will in further studies be investigated by transmission electron microscopy and high energy X-ray diffraction in a synchrotron.

Acknowledgement

The authors gratefully acknowledge the financial support from the National Natural Science Foundation of China (Grant No. 51571070, 51571071), the Scientific Research Foundation for the Returned Overseas Chinese Scholars, State Education Ministry and the Danish National Research Foundation (Grant No. DNRF86-5). Author Y.D. also gratefully acknowledges the financial support from China Scholarship Council (Grant No. 201406120134), and Gitte Christiansen for preparation of the TEM specimens.

References

[1] G.S. Cole, A.M. Sherman, Light weight materials for automotive applications, Mater. Charact. 35(1) (1995) 3-9.

[2] J. Hirsch, T. Al-Samman, Superior light metals by texture engineering: Optimized aluminum and magnesium alloys for automotive applications, Acta Mater. 61 (2013) 818-843.

[3] C. Ortiz, M.C. Boyce, Bioinspired structural materials, Science 319 (2008) 1053-1054.

[4] G.P. Chaudhari, V. Acoff, Cold roll bonding of multi-layered bi-metal laminate composites, Compos. Sci. Technol. 69 (2009) 1667-1675.

[5] B.X. Liu, L.J. Huang, X.D. Rong, L. Geng, F.X. Yin, Bending behaviors and fracture characteristics of laminated ductile-tough composites under different modes, Compos. Sci. Technol. 126 (2016) 94-105.

[6] L.J. Huang, L. Geng, H.X. Peng, Microstructurally inhomogeneous composites: Is a homogeneous reinforcement distribution optimal, Prog. Mater. Sci. 71 (2015) 93-168.

[7] L.J. Huang, S. Wang, L. Geng, B. Kaveendran, H.X. Peng, Low volume fraction in situ (Ti_5Si_3 + Ti_2C)/Ti hybrid composites with network microstructure fabricated by reaction hot pressing of Ti-SiC system, Compos. Sci. Technol. 82 (2013) 23-28.

[8] Q.S. Pan, Q.H. Lu, L. Lu, Fatigue behavior of columnar-grained Cu with preferentially oriented nanoscale twins, Acta Mater. 61 (2013) 1383-1393.

[9] X.C. Liu, H.W. Zhang, K. Lu, Strain-induced ultrahard and ultrastable nanolaminated structure in nickel, Science 342 (2013) 337-340.

[10] Y. Wei, Y. Li, L. Zhu, Y. Liu, X. Lei, G. Wang, X. Wu, Z. Mi, J. Liu, H. Wang, H. Gao, Evading the strength-ductility trade-off dilemma in steel through gradient hierarchical nanotwins, Nat. Commun. 5 (2014) 3580-3587.

[11] S. Deville, E. Saiz, R.K. Nalla, A.P. Tomsia, Freezing as a path to build complex composites, Science 311 (2006) 515-518.

[12] Z. Li, Q. Guo, Z. Li, G. Fan, D.B. Xiong, Y. Su, J. Zhang, D. Zhang, Enhanced mechanical properties of graphene (reduced graphene oxide)/aluminum composites with a bioinspired nanolaminated structure, Nano Lett. 15 (2015) 8077-8083.

[13] D.R. Lesuer, C.K. Syn, O.D. Sherby, J. Wadsworth, J.J. Lewandowski, W.H. Hunt, Mechanical behaviour of laminated metal composites, Int. Mater. Rev. 41(5) (1996) 169-197.

[14] O.D. Sherby, S. Lee, R. Koch, T. Sumi, J. Wolfenstine, Multilayered composites based on ultrahigh carbon steel and brass, Mater. Manuf. Process. 5(3) (1990) 363-373.

[15] S. Lee, J. Wadsworth, O.D. Sherby, Tensile properties of laminated composites based on ultrahigh carbon steel, J. Compos. Mater. 25 (1991) 842-853.

[16] M. Göken, H.W. Höppel, Tailoring nanostructured, graded, and particle-reinforced Al

laminates by accumulative roll bonding, Adv. Mater. 23 (2011) 2663-2668.

[17] E. Emadoddin, M. Tajally, M. Masoumi, Damping behavior of Al/SiCp multilayer composite manufactured by roll bonding, Mater. Des. 42 (2012) 334-338.

[18] H. Yu, C. Lu, A. Kiet Tieu, A. Godbole, L. Su, Y. Sun, M. Liu, D. Tang, C. Kong, Fabrication of ultra-thin nanostructured bimetallic foils by accumulative roll bonding and asymmetric rolling, Sci. Rep. 3 (2013) 2373-2381.

[19] C.Y. Liu, B. Zhang, P.F. Yu, R. Jing, M.Z. Ma, R.P. Liu, Microstructures and mechanical properties of Al/Zn composites prepared by accumulative roll bonding and heat treatment, Mater. Sci. Eng. A 580 (2013) 36-40.

[20] J.S. Carpenter, S.C. Vogel, J.E. LeDonne, D.L. Hammon, I.J. Beyerlein, Bulk texture evolution of Cu-Nb nanolamellar composites during accumulative roll bonding, Acta Mater. 60 (2012) 1576-1586.

[21] H.P. Ng, T. Przybilla, C. Schmidt, R. Lapovok, D. Orlov, H. Höppel, M. Göken, Asymmetric accumulative roll bonding of aluminium-titanium composite sheets, Mater. Sci. Eng. A 576 (2013) 306-315.

[22] A.G. Kolesnikov, A.I. Plokhikh, Y.S. Komisarchuk, I.Y. Mikhaltsevich, A study of special features of formation of submicro- and nonosize structure in multilayer materials by the method of hot rolling, Met. Sci. Heat Treat. 52 (2010) 273-278.

[23] H. Lu, X. Yuan, W. Cui, X. Ning, K. Chen, Rolling temperature on the SHS reaction of rolled Al/Ni reactive multilayer foils, Key Eng. Mater. 519 (2012) 104-107.

[24] T.I. Tabatchikova, A.I. Plokhikh, I.L. Yakovlev, S.Y. Klyueva, Structure and properties of a steel-based multilayer material produced by hot pack rolling, Phys. Met. Metallogr. 114 (2013) 580-592.

[25] J.C. Pang, G.H. Fan, X.P. Cui, A.B. Li, L. Geng, Z.Z. Zheng, Q.W. Wang, Mechanical

properties of Ti-(SiC_p/Al) laminated composite with nano-sized $TiAl_3$ interfacial layer synthesize by roll bonding, Mater. Sci. Eng. A 582 (2013) 294-298.

[26] Y. Du, G.H. Fan, T. Yu, N. Hansen, L. Geng, X. Huang, Effects of interface roughness on the annealing behaviour of laminated Ti-Al composite deformed by hot rolling, IOP Conf. Series: Materials Science and Engineering 89 (2015) 012021.

[27] L.M. Peng, J.H. Wang, H. Li, J.H. Zhao, L.H. He, Synthesis and microstructural characterization of Ti-Al_3Ti metal-intermetallic laminate (MIL) composites, Scr. Mater. 52 (2005) 243-248.

[28] E.W. Hart, Theory of the tensile test, Acta Metall. 15 (1967) 351-355.

[29] A. Dwivedi, J. Bradley, Mechanical response of titanium aluminide ($TiAl_3$), Army Research Laboratory 2010 ARL-CR-0669.

[30] J.C. Pang, X.P. Cui, A.B. Li, G.H. Fan, L. Geng, Z.Z. Zheng, Q.W. Wang, Effect of solid solution of Si on mechanical properties of $TiAl_3$ based on the multi-laminated Ti-(SiC_p/Al) composite system, Mater. Sci. Eng. A 579 (2013) 57-63.

[31] M.F. Ashby, The deformation of plastically non-homogeneous materials, Philos. Mag. 21 (1970) 399-424.

[32] M. Ma, P. Huo, W.C. Liu, G.J. Wang, D.M. Wang, Microstructure and mechanical properties of Al/Ti/Al laminated composites prepared by roll bonding, Mater. Sci. Eng. A 636 (2015) 301-310.

[33] S.B. Lee, J.E. LeDonne, S.C.V. Lim, I.J. Beyerlein, A.D. Rollett, The heterophase interface character distribution of physical vapor-deposited and accumulative roll-bonded Cu-Nb multilayer composites, Acta Mater. 60 (2012) 1747-1761.

[34] J. Wang, I.J. Beyerlein, N.A. Mara, D. Bhattacharyya, Interface-facilitated deformation twinning in copper within submicron Ag-Cu multilayered composites, Scr. Mater. 64 (2011)

1083-1086.

[35] X. Wu, P. Jiang, L. Chen, F. Yuan, Y. Zhu, Extraordinary strain hardening by gradient structure, PNAS 111 (2014) 7197-7201.

[36] M. Yang, Y. Pan, F. Yuan, Y. Zhu, X. Wu, Back stress strengthening and strain hardening in gradient structure, Mater. Res. Lett. 4 (2016) 145-151.

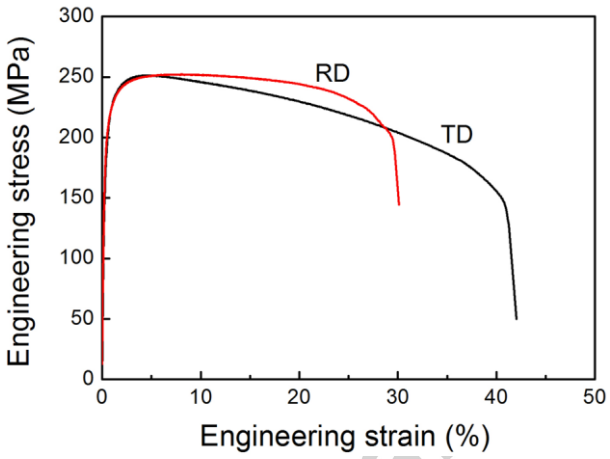

Fig. 1 Tensile engineering stress-strain curves of R100 tested in RD and TD

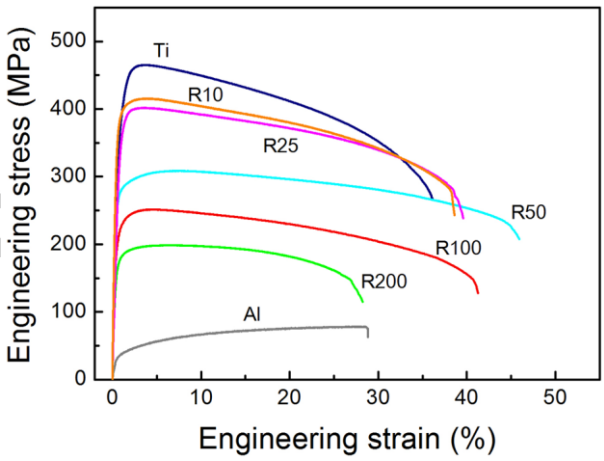

Fig. 2 Tensile engineering stress-strain curves of hot-rolled Ti and Al, and the LMCs (the loading direction is parallel to the TD)

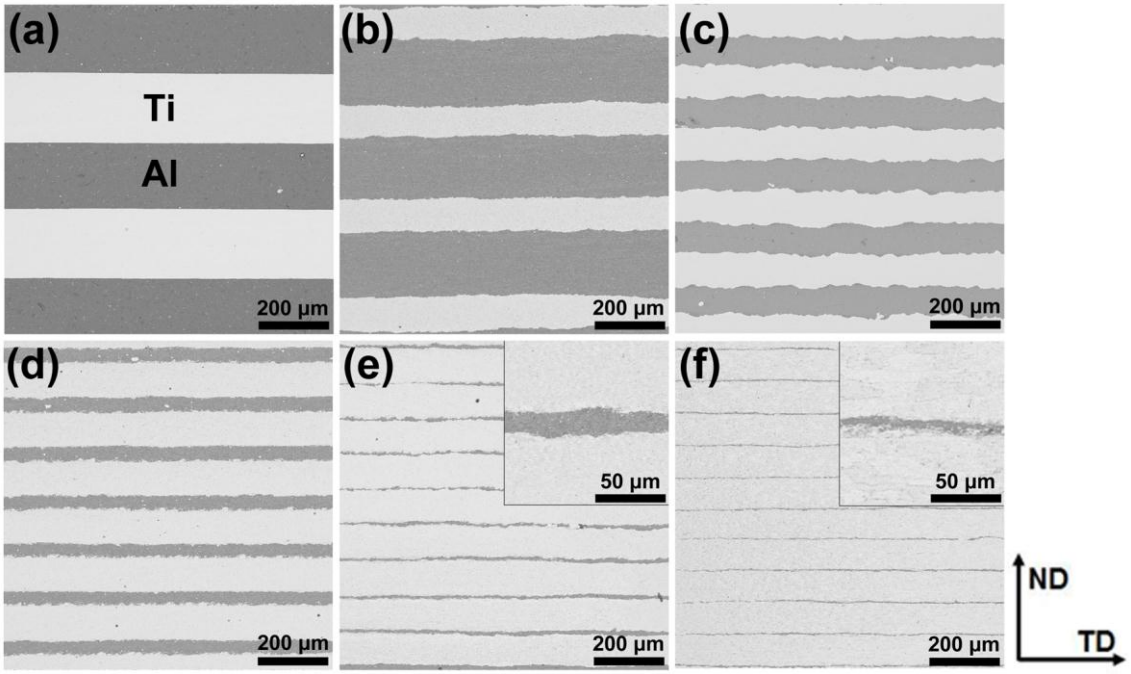

Fig. 3 BSE images of the ND-TD section of hot-pressed and hot-rolled LMCs: (a) hot-pressed Ti-Al with both Ti and Al layer thickness of 200 μm; (b) R200; (c) R100; (d) R50; (e) R25 (high magnification image in inset); (f) R10 (high magnification image in inset), showing that Ti and Al deform almost uniformly but flat interfaces become rough after hot rolling

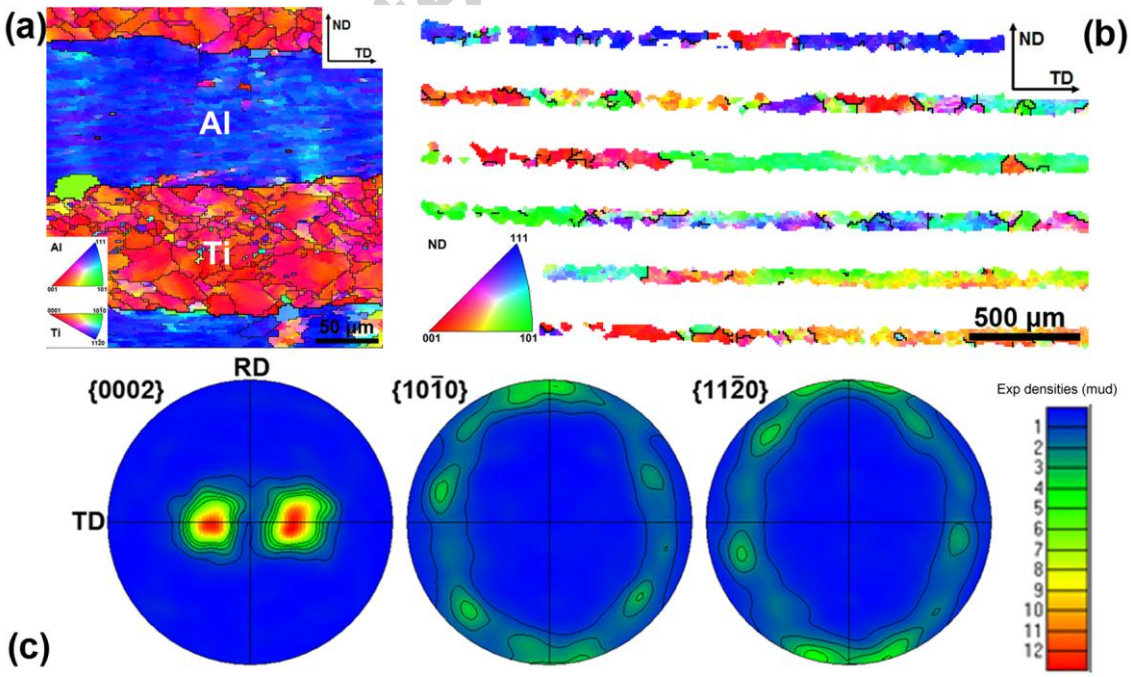

Fig. 4 An example of microstructure and texture of the LMCs (R100): (a) EBSD map of R100 (inverse pole figure of the ND); (b) EBSD map of Al layers (inverse pole figure of the ND); (c) pole figures of the Ti layer

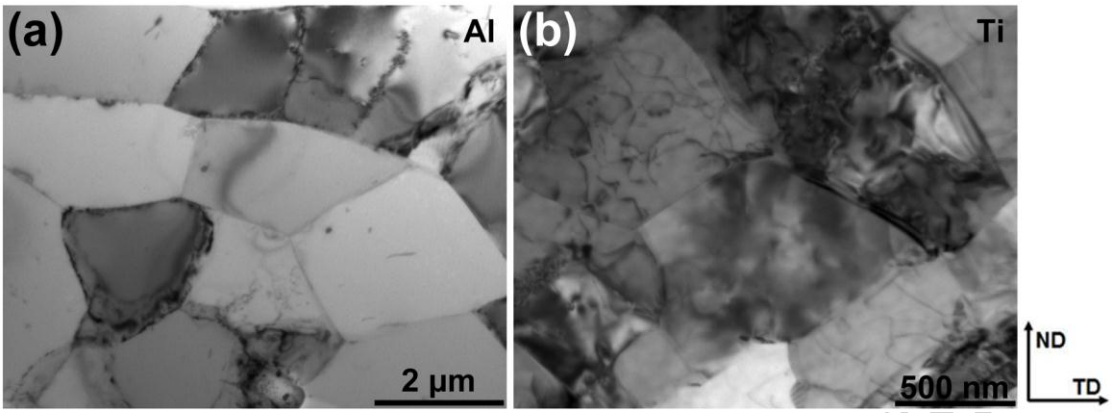

Fig. 5 Microstructure of Al and Ti in a LMC (R100) observed by TEM: (a) Al and (b) Ti. The microstructure is subdivided by sub-grain boundaries and dislocation cell boundaries (see text).

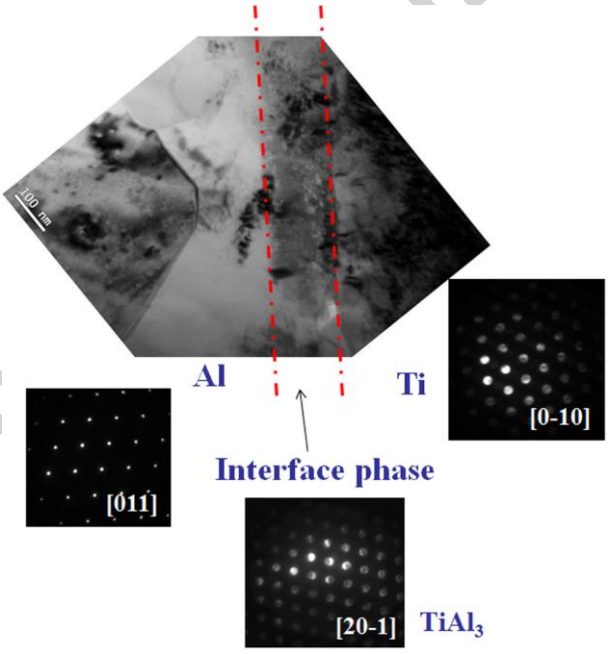

Fig. 6 Microstructure of LMC (R100) observed by TEM (bright field, selected area diffraction and micro-diffraction), showing $TiAl_3$ interface layer with a thickness about 100 nm between Ti and Al layers

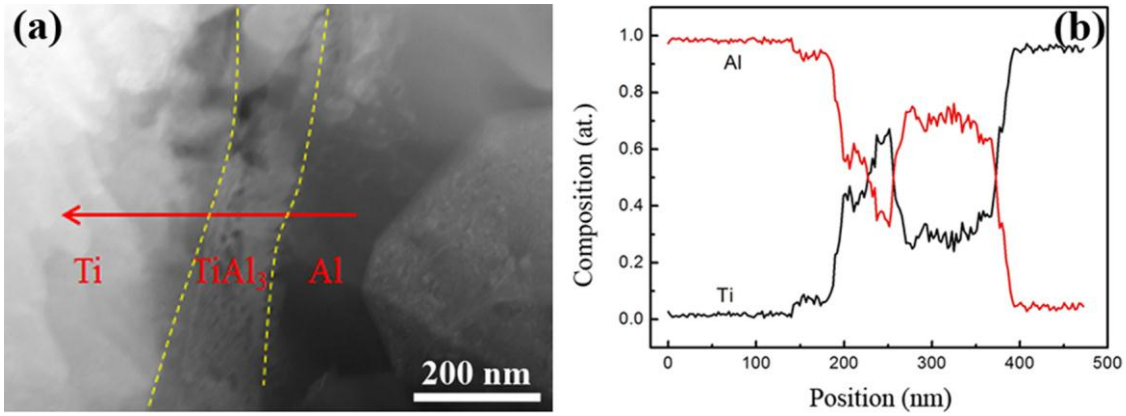

Fig. 7 EDS line scanning result at the interface region of R100: (a) microstructure in STEM mode with the $TiAl_3$ interface marked by yellow dash lines and a red arrow representing the scanning direction and position; (b) composition gradient distribution of the LMC corresponding to the red marker in (a)

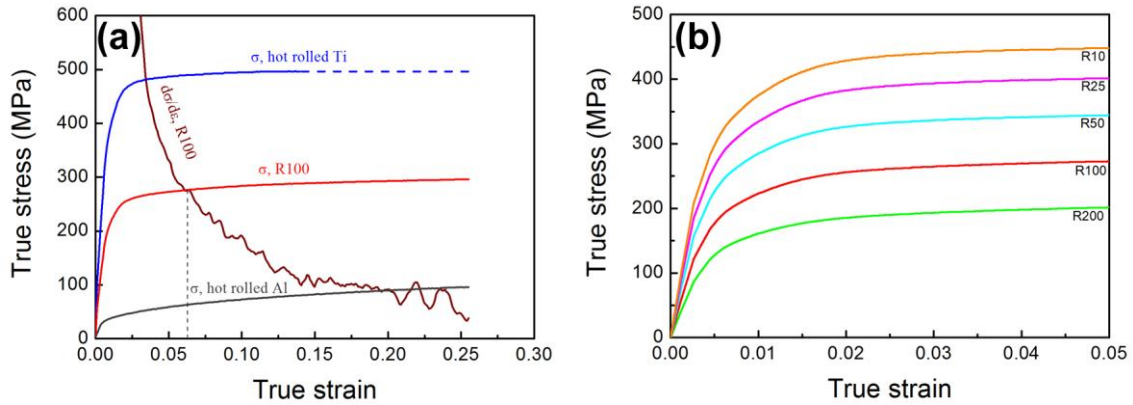

Fig. 8 Calculated tensile curves of the LMCs based on the ROM: (a) an example showing a calculated tensile curve of R100 based on tensile curves of hot-rolled Ti and Al, the intersection between the calculated tensile curve and the work hardening curve corresponds to the uniform strain ε_u and the UTS; (b) calculated tensile curves of the LMCs

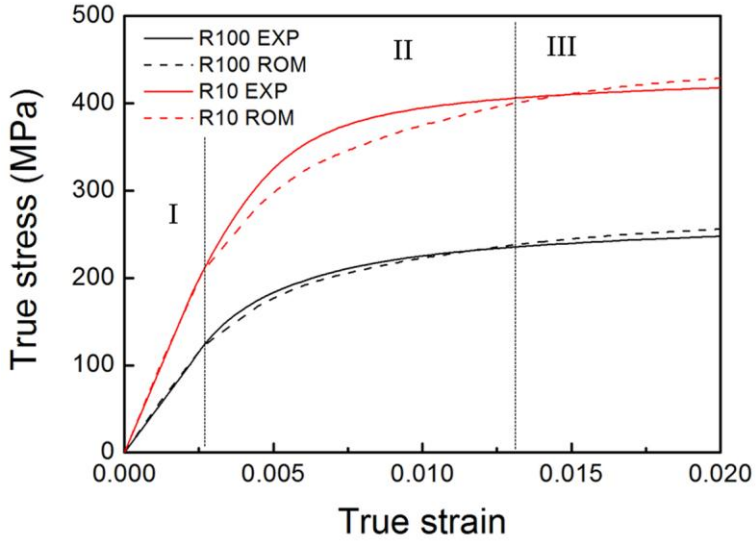

Fig. 9 Comparison between experimental and calculated results based on the ROM of the LMCs (R100 and R10 along the TD)

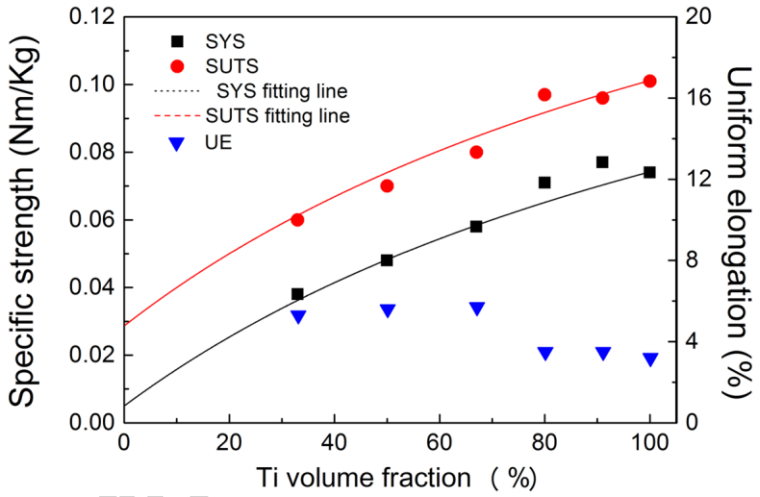

Fig. 10 Experimental results of specific strength (SYS and SUTS) and uniform elongation of hot-rolled laminated Ti-Al composites compared with the calculated specific strength (Eq. 5)

Table 1 Chemical compositions of the raw materials (wt.%)

Materials	Ti	Al	Fe	O	H	N	C	Si	Mn	Mg	Zn	Cu
TA1	Bal.	- -	0.25	0.2	0.015	0.03	0.10	0.011	- -	- -	- -	- -
1060 O	- -	Bal.	0.35	- -	- -	- -	- -	0.25	0.03	0.03	0.05	0.05

Table 2 Materials parameters of the raw materials

Materials	Density (g/cm^3)	Melting point (˚C)	Elastic modulus (GPa)	Hardness (HV)	Tensile strength σ_b (MPa)	Yield strength $\sigma_{0.2}$ (MPa)	Elongation (%)
TA1	4.5	1668	102	115.9	343	275	20
1060 O	2.7	660	70	22.2	69	28	43

Table 3 The materials parameters of the hot-rolled laminated Ti-Al composites

Materials	Layer thickness (μm)		Volume fraction (%)		Elastic Modulus (GPa)	Thickness ratio (Ti:Al)	Number of interfaces between Ti	Total thickness (mm)
	Ti	Al	Ti	Al				
R200	100	200	33.3	66.7	80.7	1:2	10	2.8
R100	100	100	50.0	50.0	86.0	1:1	15	2.9
R50	100	50	66.7	33.3	91.3	2:1	18	2.7
R25	100	25	80.0	20.0	95.6	4:1	22	2.7
R10	100	10	90.9	9.1	99.1	10:1	25	2.7

Table 4 The mechanical properties (average values with standard deviations) of the hot-rolled sheets of Ti and Al, and the laminated Ti-Al composites (R200, R100, R50, R25 and R10) according to the engineering stress-strain curves (loading along the TD)

Materials	YS (MPa)	UTS (MPa)	TE (%)	UE (%)
Ti	334.7±2.9	456.4±7.1	35.9±0.5	3.2±0.3
Al	13.8±0.3	78.4±4.2	30.5±1.9	25.8±0.2
R200	124.9±1.2	198.3±0.2	30.0±4.1	5.3±0.1
R100	171.9±1.2	250.3±3.9	40.2±1.7	5.6±0.2
R50	227.7±1.7	310.8±1.8	42.5±3.0	5.7±0.2
R25	295.3±2.0	402.7±0.1	39.4±0.3	3.5±0.1
R10	334.9±2.6	415.7±5.9	39.1±0.7	3.5±0.2

Table 5 Comparison between calculated and experimental mechanical properties of the LMCs

Materials	YS (MPa)			UTS (MPa)		
	Calculated	Experimental	Difference	Calculated	Experimental	Difference
R200	120.7	124.9	4.2	204.4	208.8	4.4
R100	174.2	171.9	-2.3	267.4	264.3	-3.1
R50	227.2	227.7	0.5	330.4	328.5	-1.9
R25	270.5	295.3	24.8	396.3	416.8	20.5
R10	305.5	334.9	29.4	422.1	430.2	8.1

Table 6 Estimation of the maximum contributions from the $TiAl_3$ layers

Materials	Volume fraction of $TiAl_3$	Contribution from $TiAl_3$ (MPa)
R200	0.00036	2.38±0.11
R100	0.00052	3.43±0.16
R50	0.00068	4.49±0.20
R25	0.00081	5.35±0.24
R10	0.00091	6.01±0.27

Table 7 Tensile specific strengths of the hot-rolled laminated Ti-Al composites

Materials	Specific YS (Nm/Kg)	Specific UTS (Nm/Kg)	ρ(g·cm^{-3})
R200	0.038	0.060	3.30
R100	0.048	0.070	3.60
R50	0.058	0.080	3.90
R25	0.071	0.097	4.14
R10	0.077	0.096	4.33